Mechanical Response of Thin Composite Beams Made of Functionally Graded Material Using Finite Element Method

Khaled Boumezbeur[1]*, Mourad Khebizi[1], Mohamed Guenfoud[2], Ilies Guendouz[2]

[1] Laboratory of Materials and Durability of Constructions, Frères Mentouri University, Constantine, 25000, Algeria
[2] Civil Engineering and Hydraulic Laboratory, University of 8 Mai 1945, P.B. 401, Guelma, 24000, Algeria
* Corresponding author, e-mail:

Abstract

Functionally Graded Material (FGM) is a new generation of composite materials, it can be used for different engineering fields according to the loading environment, but the study of its mechanical behavior requires sophisticated numerical and analytical models. Several investigations in these models are available in the literature, however, most of those investigations are based on simplifying assumptions. In this paper, we present a three-dimensional finite element modeling of functionally graded material (FGM) beams subjected to static loading. Material properties are assumed to vary continuously along the beam thickness according to the power-law distribution with linear elastic behavior. The FGM beams are discretized by hexahedral finite elements type C3D20R (continuum stress/displacement, three-dimensional 20-node, reduced integration). We studied several numerical examples of FGM beams and compare the obtained numerical results with those of analytical models in the literature.

Keywords

FGM beams, modeling, finite element method, bending behavior, static loading

1 Introduction

Classical composites made of two or more materials have been employed a lot to meet high-performance requirements. However, due to the mismatch of components, stress singularities in such composites can appear at the interface between two different materials. A large disparity in thermal expansion coefficients will lead to high residual pressures, especially in a high-temperature environment, such as the combustion chamber of an aircraft engine or a nuclear fusion reaction container [1]. As a result, the composite may experience delamination or cracking. The concept of functionally graded material was introduced to meet the demands of an environment with extremely high temperatures and eliminate stress singularities [2, 3]. The functionally graded material can be produced by continuously changing the constituents of multi-phase materials in a predetermined profile of the constituent material. Because the characteristics of FGMs change continuously, the interfaces between two materials disappear but the characteristics of two or more different materials of the composite are preserved, and therefore their fatigue properties are improved. These materials are designed to improve and optimize the thermo-mechanical

characteristics of structures at different scales. Most FGM families are gradually composed of a refractory ceramic to metal [4, 5].

The ceramic in the FGM protects against thermal effects and protects the metal against corrosion and oxidation, as the FGM is hard and reinforced by the metal composition. These materials have recently received a lot of attention because of their advantages, such as reducing material property disparities and thermal stresses, as well as their use and growth in the fields of aeronautics and aerospace, where they can serve as thermal barriers due to their rich ceramic compositions. FGMs are used in a variety of fields, including medicine, the automotive industry, military equipment, electricity, and nuclear power [6, 7]. FGMs are also being developed for general use as structural members in extremely hot environments.

Due to the increasing use of functionally graded materials in many fields and applications, many studies have been carried out on the mechanical and thermal behavior of FGMs [8, 9], in-depth theoretical and experimental studies have been carried out and published on fracture mechanics [10, 11], the distribution of thermal stresses [12, 13] and

the treatment of cracks in FGM structures [14, 15]. Among FGM structures are the beams that represent a major focus for researchers due to their applications [16].

Several approaches, have been used, including the energy method, the finite element method, and the shear strain beam theory. The majority of these approaches are predicated on simplifying assumptions [17–19].

The higher-order shear deformation theory «HSDT» has been employed by Li et al [20] for studying static bending and dynamic response of FGM beams. A finite element model (FEM) and Navier solutions are developed by Vo et al. [21], additionally they used the quasi-3D theory to determine the displacement and stresses of FG sandwich beams for various power-law index, skin-core-skin thickness ratios and boundary conditions.

A new 2-node beam element based on Quasi- 3D beam theory and mixed formulation is developed by Nguyen et al. [22] for studying static bending of functionally graded (FG) beams, the proposed beam element's transverse shear strains and stresses have parabolic distributions throughout its thickness, and the transverse shear stresses disappear on the top and bottom surfaces of the beam. The proposed beam element is shear-free and does not use selective or reduced integration.

Chikh [23] developed various higher order theories for bending of FG beams using hyperbolic shear deformation beams. These theories are developed as a function of the assumption of constant transverse displacement and variation in axial displacement of the higher-order through the thickness of the beam, and they satisfy the zero stress on the top and bottom surfaces of the beam, eliminating the need for a shear adjustment factor.

Khebizi et al. [24] recently investigated the mechanical behavior of FGM beams using a three-dimensional modeling method based on Saint Venant's exact theory, which takes into account the deformation of the FGM beam section. Guendouz et al. [25] studied the bending-torsional behavior of FGM cantilever beams using a refined beam theory (RBT). Boumezbeur et al. [26] have studied the response of FGM beams subjected to static and cyclic loading using finite element numerical modeling. Bhandari and Sharma [27] investigated thin and thick beams in terms of temperature, displacements, and stresses using a unified formulation, offering many one-dimensional displacements-based beam models that could be easily translated into higher-order theories, classical Euler-Bernoulli and Timoshenko models, although the thermo-mechanical problems studied offer global bending deformation,

they are governed by three-dimensional stress fields that call for very accurate models. Althoey and Ali [28] presented a streamlined method and solution for FGM beam normal and shear stress analysis based on two material functions: power-law (P-FGM) and exponential (E-FGM). Furthermore, the influence of material functions on FGM beam deflection has been investigated using analytical solutions involving simply supported and cantilever FGM beams, which exhibited less deformation when compared to homogenous steel beams of the same size and loadings, they concluded from their findings that the non-dimensional normal stress and shear stress in the E-FGM material function model are independent of the elastic modulus values of the constituent materials, but rather depend on both the ratio of the elastic modulus and the location across the beam thickness. Nguyen et al. [29] used large deflection analysis of functionally graded beams based on geometrically exact three-dimensional beam theory and isogeometric analysis to model the spatial behavior of the beams under different loading conditions, with five standard benchmark test cases carried out to validate the accuracy and efficiency of the proposed approach. Guendouz et al. [30, 31] Presented a bending-torsional behavior analysis of the functionally graded materials (FGMs) cantilever beams (I-section, U-section and square-section) were studied using a refined 1D/3D beam theories (RBT, RBT* and RBTd based on the 3D Saint Venant's solution).

The size-dependent wave dispersion in FG GPLs reinforced bi-layer nanobeams embedded in Pasternak elastic foundation and subjected to an axial compressive mechanical load and axial magnetic field is investigated by Zenkour and Sobhy [32]. Giunta et al. [33] proposed several axiomatic refined theories for the linear static analysis of FGM beams whose properties are graded along one or two directions, as these beams are subjected undergo bending and torsional loadings. Zghal et al. [34] presented a first attempt to explore the influence of porosity on bending static analysis of functionally graded (FG) beams using a refined mixed finite element beam model, where a parametric study was carried out to show the effects of power law index, porosity coefficient, boundary conditions and types of porosity distributions on deflections and stresses of the studied FG beams.

In this study, we present a three-dimensional modeling of the static response of FGM beams using the finite element method, in which the FGM beams are modeled by hexahedral elements type C3D20R. Numerical results are compared with those predicted by other theories and

analytical models in the literature to show the effects of the power-law index on the flexural response and stresses of the FG beams are investigated.

2 Modeling of FGM beam

FGMs are composed of two or more materials that have various structural and functional qualities, and the mechanical properties of these elements are optimally dispersed to enhance the performance of their overall structure. FGMs are often made of a combination of metal and ceramic (Fig. 1). The low thermal conductivity of the ceramic component provides resistance to high temperatures. On the other hand, the ductile metal component resists fracture in a remarkably short time when subjected to stresses caused by a high-temperature gradient. FGMs are distinguished by their non-uniform microstructures and macro-properties that graduate in space. The variation of the volume fractions can be used to characterize how gradually and continuously their mechanical properties change from one surface to another across the thickness of the beam.

Many approaches exist in the literature [19, 24, 35, 36] for the computation of Young's modulus $E(z)$ and Poisson's ratio $v(z)$, we have the distribution of the power-law functions (P-FGM), exponential functions (E-FGM), Mori Tanaka functions (M-FGM) and sigmoid functions (S-FGM).

In the study of Khebizi et al. [24], the distribution methods of the mechanical properties of FGM beams are presented in detail.

In this work, the material properties of a P-FGM, such as Young's modulus $E(z)$ can be determined by the law of mixtures as following:

$$E(z) = (E_c - E_m)V_c(z) + E_m ,\tag{1}$$

where E_c and E_m are respectively the Young's modulus at the top ($z = +h/2$) and bottom ($z = -h/2$) surfaces of the FGM beam, $V_c(z)$ is the volume fraction of the P-FGM class, it obeys a power law function according to the following equation:

$$V(z) = \left(\frac{z}{h} + \frac{1}{2}\right)^p ,\tag{2}$$

where $p(0 \leq p \leq \infty)$ is a variable parameter (is the volume fraction index) that dictates material variation profile through the thickness and z is the distance from the midplane of the FG beam.

The volume fractions of the metal (V_m) and the ceramic (V_c) constituents related by:

$$V_c + V_m = 1\tag{3}$$

Hence, from Eqs. (1), (2) and (3), The FG beam becomes a fully ceramic beam when p is set to be zero, whereas infinite p indicates a fully metallic beam.

Fig. 2 clearly illustrates how the volume fraction for $p < 1$ changes quickly near the bottom surface and quickly increases for $p > 1$ near the top surface of FGM beams.

For the present FGM beam model, the top beam surface ($z = +h/2$) is purely ceramic and the bottom beam surface ($z = -h/2$) is purely metal. It is to be mentioned that the subscripts m and c refer to the metal and ceramic constituents respectively.

Poisson's ratio has a very small impact on strain when compared to Young's modulus. Therefore, Poisson's ratio can be assumed to be constant (Khebizi et al. [24], Guenfoud et al. [35], Hadji et al. [36], Delale and Erdogan [37], Ben-Oumrane et al. [38]).
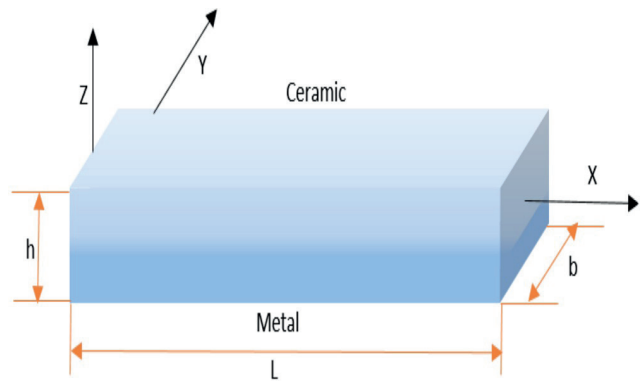

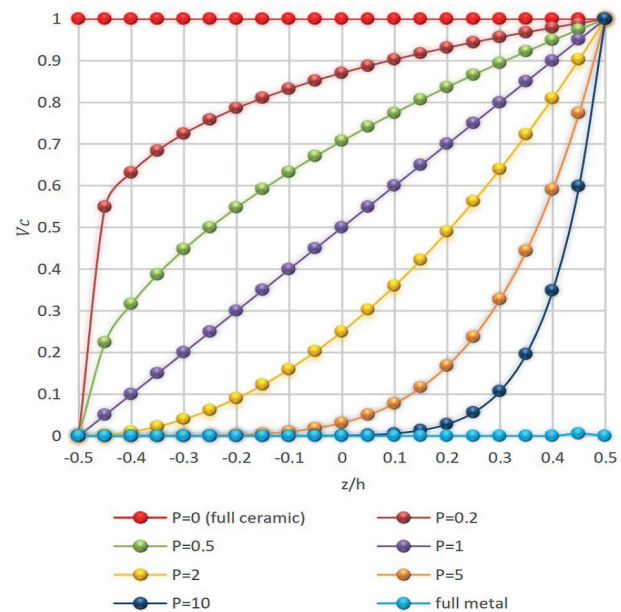**Fig. 1** FGM beam with dimensions and coordinate axes

Fig. 2 Variation of volume fraction of FGM beam along the thickness for various power law indexes

3 Mathematical formulation of C3D20R finite element

In the present work, the twenty-node brick element (C3D20R) with reduced integration points ($3 \times 3 \times 3$) is used (Fig. 3), where and despite the reduced integration, this element behaves very well in bending and rarely displays hourglassing. According to Dhondt [39], the displacement of each element is a continuous function of the nodal displacement utilizing the shape functions of displacement and geometry.

In traditional finite element formulations, each element is given a preset set of material properties, ensuring that the property field is constant inside each individual element. The material's property function must be discretized in accordance with the element's mesh size in order to model a continuously non-homogeneous material.

The formulation provided by Smith [40] indicates that this approach can produce significant discontinuities. The assumption of constant properties for each element may result in inaccurate conclusions because each Gaussian point of the element has its own stress-strain curve in the elastic analysis of FGMs. The graded finite element is therefore far superior for modeling issues with non-homogeneous materials. According to Zafarmand and Kadkhodayan [41], second order three-dimensional continuum (solid) elements should be taken into account while doing a 3D elastic analysis. These elements are excellent in bending-dominated issues and offer higher accuracy than first-order ones for smooth situations that do not entail severe element distortions. A hexahedral C3D20R element's local domain is a cube that spans from −1 to +1 ($-1 \leq g, h, r \leq 1$) along each coordinate axis. This element has 20 nodes, which are distributed evenly along the edges and at the vertices as illustrated in Fig. 3. According to Smith's [40] description of the Abaqus node numbering standard, for second-order elements, the corner nodes are numbered first, followed by the midside nodes as also illustrated in Fig. 3. Additionally, it has been demonstrated by Liew and Rajendran [42] that the decreased integration

locations are the so-called superconvergent point, where the stress is one order more accurate than at any other point. But with less integration, so-called zero-energy modes might appear and produce hourglassing.

Based on the study of Smith [40]. The interpolation function is given as below:

$$
\begin{aligned}
u = &-\frac{1}{8}(1-g)(1-h)(1-r)(2+g+h+r)u_1 \\
&-\frac{1}{8}(1+g)(1-h)(1-r)(2-g+h+r)u_2 \\
&-\frac{1}{8}(1+g)(1+h)(1-r)(2-g-h+r)u_3 \\
&-\frac{1}{8}(1-g)(1+h)(1-r)(2+g-h+r)u_4 \\
&-\frac{1}{8}(1-g)(1-h)(1+r)(2+g+h-r)u_5 \\
&-\frac{1}{8}(1+g)(1-h)(1+r)(2-g+h-r)u_6 \\
&-\frac{1}{8}(1+g)(1+h)(1+r)(2-g-h-r)u_7 \\
&-\frac{1}{8}(1-g)(1+h)(1+r)(2+g-h-r)u_8 \\
&+\frac{1}{4}(1-g)(1+g)(1-h)(1-r)u_9 \\
&+\frac{1}{4}(1-h)(1+h)(1+g)(1-r)u_{10} \\
&+\frac{1}{4}(1-g)(1+g)(1+h)(1-r)u_{11} \\
&+\frac{1}{4}(1-h)(1+h)(1-g)(1-r)u_{12} \\
&+\frac{1}{4}(1-g)(1+g)(1-h)(1+r)u_{13} \\
&+\frac{1}{4}(1-h)(1+h)(1+g)(1+r)u_{14} \\
&+\frac{1}{4}(1-g)(1+g)(1+h)(1+r)u_{15} \\
&+\frac{1}{4}(1-h)(1+h)(1-g)(1+r)u_{16} \\
&+\frac{1}{4}(1-r)(1+r)(1-g)(1-h)u_{17} \\
&+\frac{1}{4}(1-r)(1+r)(1+g)(1-h)u_{18} \\
&+\frac{1}{4}(1-r)(1+r)(1+g)(1+h)u_{19} \\
&+\frac{1}{4}(1-r)(1+r)(1-g)(1+h)u_{20}
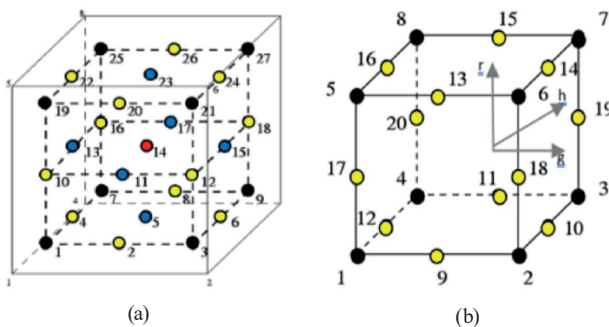\end{aligned}
\tag{4}
$$

Fig. 3 hexahedral finite element (C3D20R); (a) Hexahedral C3D20R components with a $3 \times 3 \times 3$ integration point arrangement, (b) Twenty nodes of C3D20R element

Reduced integration is used to numerically integrate each isoparametric solid element. Gauss integration is utilized for the second-order elements because it is effective and particularly suitable for the polynomial product interpolations employed in these elements. The interpolation function given in Eq. (4) can be expressed as follows for the 20-node brick elements:

$$\boldsymbol{u} = N^I(g,h,r)\boldsymbol{u}^I \text{ sum on } I. \tag{5}$$

The isoparametric shape functions can be written as (Smith [40]):

$$N^I(g,h,r) = 1/8\Sigma^I + 1/4g\Lambda_1^I + 1/4h\Lambda_2^I + 1/4r\Lambda_3^I$$
$$+1/2hr\Gamma_1^I + 1/2gr\Gamma_2^I + 1/2gh\Gamma_3^I + 1/2ghr\Gamma_4^I, \tag{6}$$

where:

$$\Sigma^I = \left[+1,+1,+1,+1,+1,+1,+1,+1\right],$$
$$\Lambda_1^I = \left[-1,+1,+1,-1,-1,+1,+1,-1\right],$$
$$\Lambda_2^I = \left[-1,-1,+1,+1,-1,-1,+1,+1\right],$$
$$\Lambda_3^I = \left[-1,-1,-1,-1,+1,+1,+1,+1\right], \tag{7}$$
$$\Gamma_1^I = \left[+1,+1,-1,-1,-1,-1,+1,+1\right],$$
$$\Gamma_2^I = \left[+1,-1,-1,+1,-1,+1,+1,-1\right],$$
$$\Gamma_3^I = \left[+1,-1,+1,-1,+1,-1,+1,-1\right],$$
$$\Gamma_4^I = \left[-1,+1,-1,+1,+1,-1,+1,-1\right],$$

and the node of the element is indicated by the superscript I. The next four vectors Γ_α^I, (has a range of four), are the hourglass base vectors, which are the deformation modes connected to no energy in the 1-point integration element but leading to a non-constant strain field in the element.

The gradient matrix B^I in the uniform strain formulation is defined by integrating across the element as follows (Smith [40]):

$$B^I = \frac{1}{V_{el}}\int_{V_{el}} N_i^I(g,h,r)dV_{el}, \tag{8}$$

$$N_i^I(g,h,r) = \frac{\partial N^I}{\partial x_i}, \tag{9}$$

where V_{el} is the element volume and i has a range of three. In the centroidal strain formulation the gradient matrix is B^I simply given as:

$$B_i^I = N_i^I(0,0,0), \tag{10}$$

which has the following antisymmetric property:

$$B_i^1 = B_i^7$$
$$B_i^3 = B_i^5$$
$$B_i^2 = B_i^8 \tag{11}$$
$$B_i^4 = B_i^6$$

The centroidal strain formulation makes it easier to compute the gradient matrix, as can be shown from Eqs. (4) to (11). Due to the gradient matrix's antisymmetric property, cost savings also apply to calculations of strain and element nodal forces. When the components are skewed, the centroidal strain formulation is less precise. According to Smith [40], the uniform strain approach and the centroidal strain approach are the same for hexahedral elements in a parallelepiped configuration.

4 Numerical results and discussions

Here we present and discuss some numerical examples to confirm the accuracy of 3D numerical modeling using the finite element method in the simulation and prediction of free bending responses of a simply supported FGM beam. In this work, the P-FGM beam is modeled using Abaqus software.

4.1 Numerical applications
4.1.1 Geometric and materiel properties of FGM beam

The present work aims at studying a simply supported FGM beam. A uniform rectangular beam with length L, height h and unit width b is considered for which the ratio between its length and height (L/h) is equal to twenty (20). A beam with symbolic dimensions is shown in Fig. 1, where, x, y and z denote the coordinate axes along the length, width and thickness directions, respectively. The bottom surface of the beam is assumed to be aluminum (Al), while its top surface is assumed to be pure alumina (Al_2O_3), this beam is made of elastic and isotropic material with material properties varying smoothly in the z thickness direction.

The various material properties of the FGM constituents are presented in Table 1.

This beam is subjected to a uniformly distributed load of $q = 10$ N/m (Fig. 4).

Table 1 Materiel properties of the FGM constituent

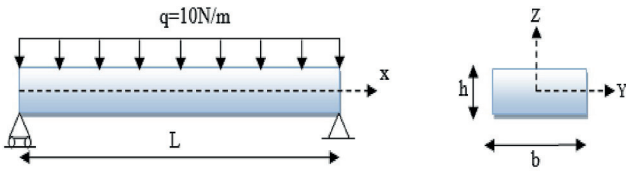| Material property	Al	Al_2O_3
E (GPa)	70	380
v	0.3	0.3

Fig. 4 Geometric characteristics and properties of the FGM beam
(*L/h* = 20) subjected to a uniformly distributed load

4.1.2 Investigation on mesh dependence/accuracy

In this section, we investigate the mesh dependence and accuracy in beam. The Finite Element Method (FEM) is used to model the beams by hexahedral elements of type C3D20R with 20 nodes and 27 integration points, and the effect of the mesh density on the accuracy of the results is examined. A series of numerical simulations are performed with different mesh densities, and the results are compared to determine the impact of the mesh density on the accuracy of the results. Our findings suggest that the accuracy of the results is significantly influenced by the mesh density, and that there is a critical mesh density beyond which further refinement does not lead to a significant improvement in the accuracy of the results. These simulations are carried out using Abaqus software. The effect of mesh density on the accuracy of results is only performed for homogeneous beams.

Fig. 5 shows five numerical simulations performed with different mesh densities. The mesh density is varied by changing the number of elements used to model the beams. The number of elements used in the simulations ranges from 300 to 60000 as shown in Table 2.

Fig. 6(a) and Table 2 show that the deflection of the homogeneous beams (full metal and full ceramic) obtained from different mesh densities is not influenced by the mesh
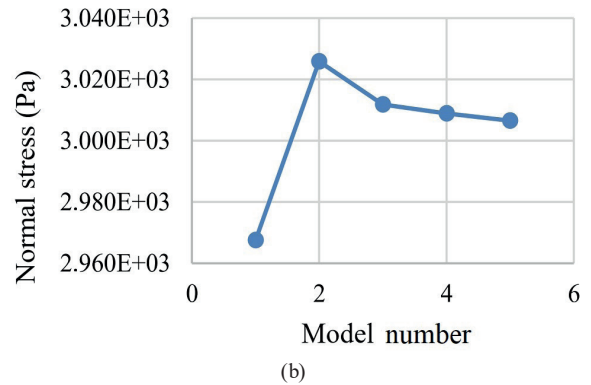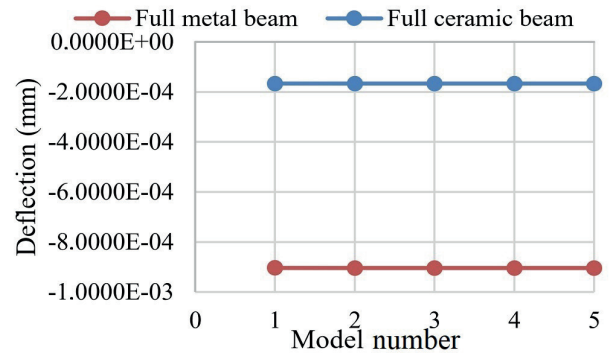

Fig. 6 Variation of the deflection and normal stress obtained for different mesh densities; (a) variation of the deflection, (b) variation of the normal stress

density. However, the normal stress is significantly influenced by the mesh density (Fig. 6(b) and Table 2). It can be noted that beyond a certain mesh density, the improvement in accuracy is marginal, for this reason we have chosen the mesh density of model 5 (Fig. 5(e)).

The three-dimensional field of vertical displacement and normal stresses field σ_{xx} of the FGM beam are shown in Figs. 7 and 8, respectively. The results of deflection along
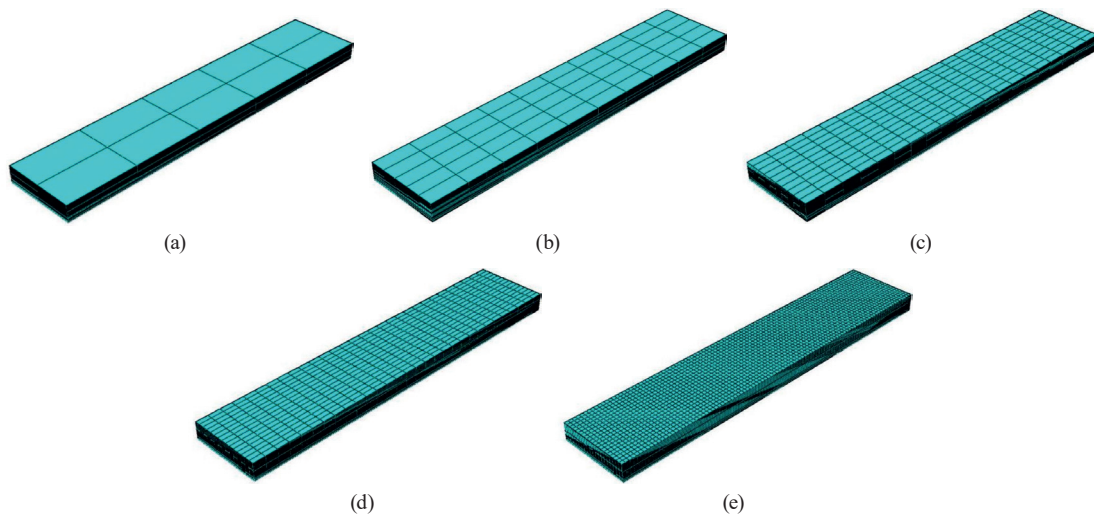

Fig. 5 Different mesh densities of the FGM beam; (a) Model 1 with 300 elements, (b) Model 2 with 1500 elements, (c) Model 3 with 6000 elements,
(d) Model 4 with 13500 elements, (e) Model 5 with 60000 elements

Table 2 Deflection and normal stress obtained for different mesh densities

Model	Mesh density	Deflection (full ceramic) (mm)	Deflection (full metal) (mm)	Normal stress (Pa)
Model 1	300 elements	-1.06649E-4	-1.06649	2.968E+3
Model 2	1500 elements	-1.06654E-4	-1.06654	3.026E+3
Model 3	6000 elements	-1.06654E-4	-1.06654	3.012E+3
Model 4	13500 elements	-1.06654E-4	-1.06654	3.009E+3
Model 5	60000 elements	-1.06654E-4	-1.06654	3.007E+3

the length of the mean- line of the beam (W), the normal stresses σ_{xx} at mid-span of the FGM beam ($x = L/2$) and the shear stresses σ_{xz} at the level of the support ($x = 0$), obtained by the finite element method, are shown in Figs. 9 and 10, respectively.

4.1.3 Discussion

The results obtained for the deflection of the FGM beam are shown in Fig. 9 for various power law exponents, p. This deflection increases as power law exponent p is increased, due to the effect of Young's modulus, which is higher for ceramics ($P = 0$) than for metals ($P = +\infty$).

As seen from Fig. 10 the variation of normal stresses σ_{xx} (Fig. 10(a)) through the thickness of the FGM beam is not linear and also the values of tensile stresses are lesser than compressive stresses. In contrast, for the isotropic beams (full-ceramic), the variation of the normal stress is linear and the value of normal stress is zero at the mid-plane but it is clearly visible that the values of normal stresses are not zero at the mid-plane of the FG beam for the other values of power law index, it indicates that the neutral plane of the beam moves towards the upper side of the beam for FG-beam. This is due to the variation of Young's modulus through the thickness of the FG beam.
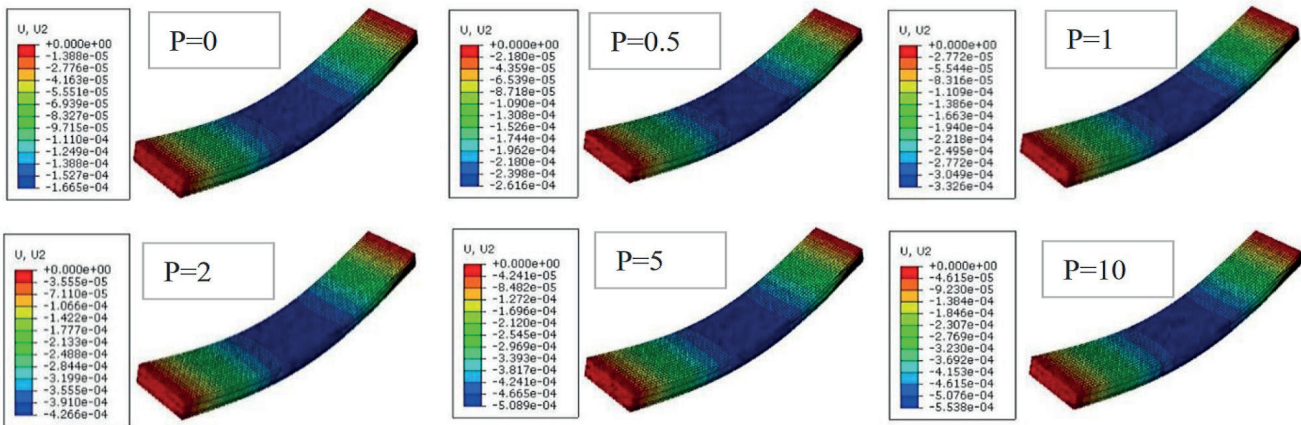

Fig. 7 Three-dimensional vertical displacement field of FGM beam obtained by Abaqus calculation code for different values of P
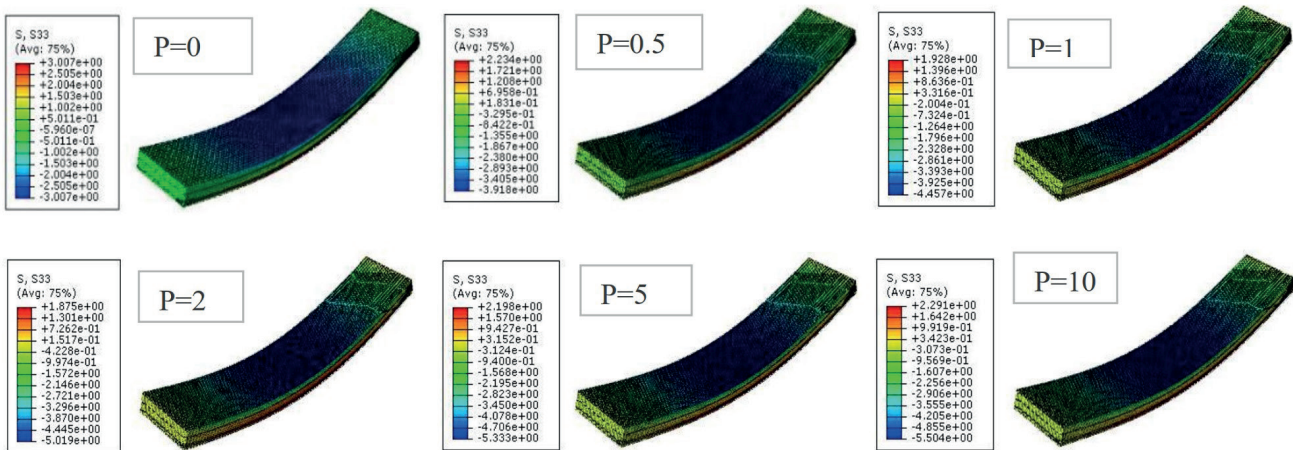

Fig. 8 Three-dimensional normal stress field σ_{xx} of FGM beam obtained by finite element method using Abaqus calculation code for different values of P
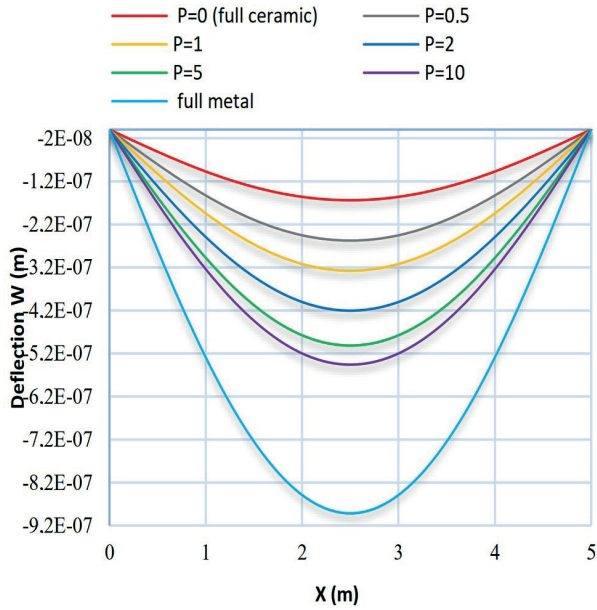
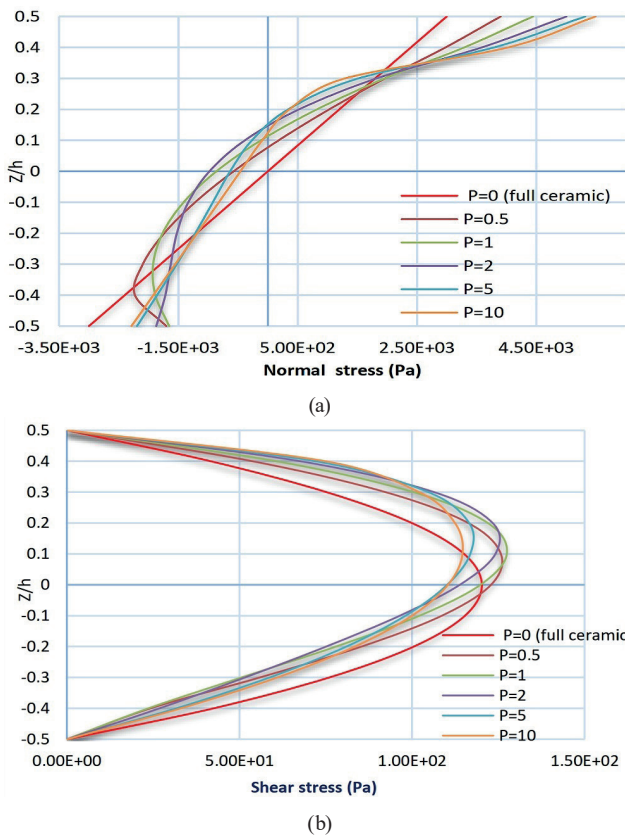**Fig. 9** Deflection along the length of the midline FGM beam

(a)

(b)

Fig. 10 Distribution of normal stresses σ_{xx} at mid-span (at $x = L/2$) and shear stresses σ_{xx} at the level of the support (at $x = 0$) through the thickness of P-FGM beam; (a) Normal stresses σ_{xx}; (b) Shear stresses σ_{xx}

Fig. 10(b) depicts the variation of the shear stress across the thickness of FGM beam. With increasing power law index p, the tip of shear stress decreases. It is observed that the distribution of the shear stresses σ_{xz}, through the

thickness of the beam is parabolic and symmetric about the neutral plane for ceramic isotropic (full ceramic or full metal) beams only, while the relative location of the neutral plane is not the same for FGM beams with different power law indexes. It is also seen that the maximum value of the shear stress is located at a point above the mid-plane for FGM beam with power law index: 0.5, 1, 2, 5 and 10.

For the validation of our numerical model in the case of bending analysis, we present these results in terms of non- dimensional quantities. For convenience, the following dimensionless forms are used:

$$Displacement \ \overline{w}\left(x = \frac{L}{2} \right) = 100 \frac{E_m h^3}{qL^4} w, \tag{12}$$

$$Normal \ stress \ \overline{\sigma}_{xx}\left(x = \frac{L}{2}, y = \frac{h}{2} \right) = \frac{h}{qL} \sigma_{xx}, \tag{13}$$

$$Shear \ stress \ \overline{\sigma}_{xz}\left(x = 0, y = 0 \right) = \frac{bh}{qL} \sigma_{xz}. \tag{14}$$

The results obtained from our model are displayed in Table 3, and for various non-dimensional displacements and stresses of FG beams under uniform load q for different values gradient index p. It can be observed that the non-dimensional deflections obtained by our model with FEM are in good correlation with the provided results by the analytical beam theories (Li et al. [20], Vo et al. [21], Nguyen et al. [22] and Chikh [23]). But we observed a discrepancy in terms of shear and especially normal stress.

As shown in Table 3, we translated the obtained results, which were compared with previous results in the literature, into graphs to demonstrate the effect of the power law index p on the behavior of FGM beams under a uniformly distributed static load.

Fig. 11 illustrates the variation in non-dimensional deflection with respect to changes in the power law index. It can be observed that as the power law index parameter is increased, the stiffness of the FGM beam decreases. This decrease in stiffness results in an increase in deflection. This figure also shows a comparison of the results on deflection obtained by the present model (with finite element method), and these obtained by analytical methods (Li et al. [20] model, model of Vo et al. with Navie's theory [21], model of Nguyen et al. with quasi-3d theory [23] and Chikh model with HPSDT [23]). As it can be seen from Fig. 11, there is a good agreement between the results obtained the present model and these obtained by analytical methods.

Table 3 Comparison of non-dimensional static deflection and stresses of FG beams under uniform load

p	Method	$\bar{w} = (x = L/2)$	$\bar{\sigma}_{xx} (x = L/2, z = h/2)$	$\bar{\sigma}_{xz} (x = 0, y = 0)$
0	Present model	2.8747	14.9902	0.6012
	Li et al. [20]	2.8962	15.013	0.75
	Vo et al. [21] with Navie's theory	2.8947	15.0125	0.7432
	Vo et al. [21] with a FEM model	2.8947	15.0200	0.7466
	Quasi-3D theory Nguyen et al. [22]	2.8938	15.0079	0.7454
	HPSDT (model 1) Chikh [23]	2.8958	15.0087	0.635
	HPSDT (model 2) Chikh [23]	2.8962	15.0129	0.7425
0.5	Present model	4.5149	19.5052	0.6145
	Li et al. [20]	4.4645	19.7005	0.7676
	Vo et al. [21] with Navie's theory	/	/	/
	Vo et al. [21] with a FEM model	/	/	/
	Quasi-3D theory Nguyen et al. [22]	/	/	/
	HPSDT (model 1) Chikh [23]	4.4638	19.6946	0.6526
	HPSDT (model 2) Chikh [23]	4.4644	19.7003	0.7595
1	Present model	5.7419	22.2093	0.5991
	Li et al [20]	5.8049	23.2054	0.75
	Vo et al [21] with Navie's theory	5.7201	23.2046	0.7432
	Vo et al [21] with a FEM model	5.7197	23.2200	0.7466
	Quasi-3D theory Nguyen et al [22]	5.7179	23.1970	0.7457
	HPSDT (model 1) Chikh, [23]	5.8041	23.1982	0.635
	HPSDT (model 2) Chikh, [23]	5.8049	23.2051	0.7425
2	Present model	7.3634	25.0128	0.5692
	Li et al. [20]	7.4415	27.0989	0.6787
	Vo et al. [21] with Navie's theory	7.2805	27.0988	0.6809
	Vo et al. [21] with a FEM model	7.2797	27.1100	0.6776
	Quasi-3D theory Nguyen et al. [22]	7.2770	27.0884	0.6828
	HPSDT (model 1) Chikh [23]	7.4403	27.0896	0.5687
	HPSDT (model 2) Chikh [23]	7.442	27.0989	0.6795
5	Present model	8.7844	26.5917	0.5509
	Li et al. [20]	8.8151	31.8112	0.579
	Vo et al. [21] with Navie's theory	8.6479	31.8137	0.6010
	Vo et al. [21] with a FEM model	8.6471	31.8300	0.6036
	Quasi-3D theory Nguyen et al. [22]	8.6435	31.7987	0.6022
	HPSDT (model 1) Chikh [23]	8.813	31.7987	0.481
	HPSDT (model 2) Chikh [23]	8.8181	31.8125	0.5988
10	Present model	9.5592	27.4563	0.5521
	Li et al. [20]	9.6879	38.1372	0.6436
	Vo et al. [21] with Navie's theory	9.5749	38.1395	0.6583
	Vo et al. [21] with a FEM model	9.5743	38.1600	0.6675
	Quasi-3D theory Nguyen et al. [22]	9.5698	38.1176	0.6595
	HPSDT (model 1) Chikh [23]	9.6856	38.1235	0.5364
	HPSDT (model 2) Chikh [23]	9.6904	38.1382	0.6563

Fig. 12 shows the stress variation obtained from the present model with FEM and analytical methods. As can be seen from this figure and the Table 3, the stress variation obtained from the analytical method is generally higher than that obtained by the FEM especially if the index
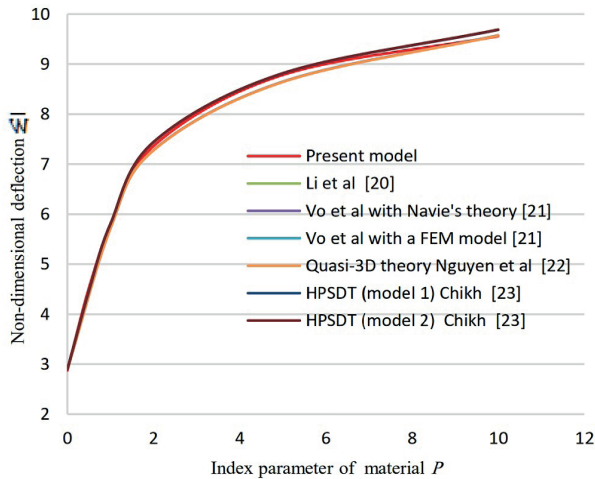

Fig. 11 Variation of non-dimensional deflection $\overline{w}$ in terms of power law index P of FGM beam
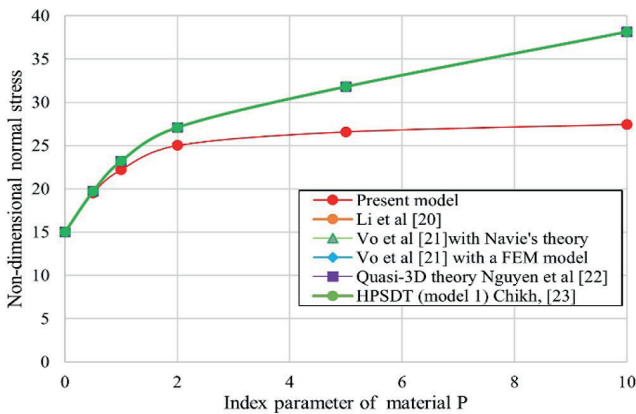

Fig. 12 Variation of non-dimensional normal stress $\overline{\sigma}_{xx}$ in terms of power law index P of FGM beam
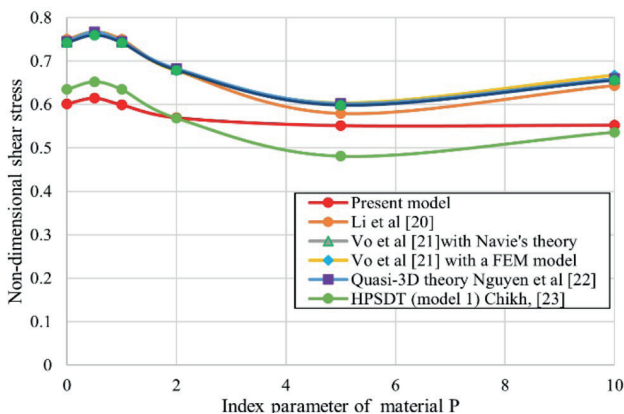

Fig. 13 Variation of non-dimensional shear stress $\overline{\sigma}_{xz}$ in function of index parameter P of FGM beam

values are greater than 2. This can be attributed to the fact that the FEM takes into account the effects of section deformations (warping, Poisson's effects, distortions and 3D behavior), which are not considered in the analytical methods and on other hand the analytical methods are based on several simplified assumptions such as those related to the kinematics of the beams. For example, Euler-Bernoulli and Timoshenko theories in which assume that the section is undeformable (for Bernoulli, the section remains, furthermore, normal to the beam axis after deformation). but the present model with FEM it is independent of any kinematic or static assumption. This method is based on a theory that allows the deformation of the section in and out of its plane via the three-dimensional modelling.

Fig. 12 shows that the results obtained by the finite element method are the only ones that have a bias compared to the results obtained by all other analytical methods.

Fig. 13 shows the non-dimensional shear stress variation obtained from the present model with FEM and analytical methods. As can be seen from the figure, the shear stress distribution obtained from the FEM is different than that obtained with analytical methods. This can be attributed to the fact that the FEM takes into account the effects of section deformations (warping, Poisson's effects, distortions and 3D behavior), which are not considered in the analytical methods. However, the difference between the FEM and analytical results is not significant, and the analytical method provides reasonable approximations for the stress distribution.

From the results shown in Table 3 and in Figs. 11, 12 and 13 we can conclude that the analytical methods have some limitations and disadvantages compared to finite element methods:

Analytical methods are generally limited to simple geometries and boundary conditions. Complex geometries and boundary conditions may require more advanced analytical methods, which can be challenging or even impossible to obtain.

Analytical solutions are based on assumptions and simplifications that may not hold in real-world situations. These assumptions can lead to inaccuracies in the solution, particularly for complex problems.

Analytical methods provide closed-form solutions that are specific to the problem being analyzed. Changing the problem's parameters, such as material properties or boundary conditions, may require a new solution to be derived.

In contrast, finite element methods have several advantages over analytical methods:

Finite element methods can handle complex geometries and boundary conditions and can be adapted to various types of problems, such as nonlinear and dynamic problems.

Finite element methods can provide accurate solutions for a wide range of problems, even with irregular geometries and boundary conditions.

Finite element methods can be combined with other numerical methods, such as optimization algorithms, to solve more complex problems.

5 Conclusions

In this paper, a hexahedral finite element type C3D20R "quadratic brick element characterized by 20 nodes with 27 integration points ($3 \times 3 \times 3$) was used for the numerical analysis of the static behavior of simply supported elastic rectangular FGM beam subjected to uniform loading, where the material properties of the FGM beams change continuously throughout the thickness of the beam, according to the volume fraction of the constituent materials based on the power law functions.

Through numerical bending applications of FGM beams, the performance, reliability and versatility of the C3D20R element were evaluated. The static study results were compared to analytical models in the literature. The static study results were compared to analytical models in the literature. These comparisons have shown that the non-dimensional deflections obtained by our model with FEM are in good correlation with the provided results by the analytical beam theories. But we observed a discrepancy in terms of shear and especially normal stress. This can be attributed to the fact that the FEM takes into account the effects of section deformations (warping, Poisson's effects, distortions and 3D behavior), which are not considered in the analytical methods and on other hand the analytical methods are based on several simplified assumptions.

As a result, our three-dimensional modeling based on C3D20R hexahedral finite elements implanted in the Abaqus calculation code was able to simulate and describe the static behavior of P-FGM beams.

References

[1] Chi, S.-H., Chung, Y.-L. "Mechanical behavior of functionally graded material plates under transverse load - Part I: Analysis", International Journal of Solids and Structures, 43(13), pp. 3657–3674, 2006.
https://doi.org/10.1016/j.ijsolstr.2005.04.011

[2] Niino, M., Maeda, S. "Recent development status of functionally gradient materials", ISIJ International, 30(9), pp. 699–703, 1990.
https://doi.org/10.2355/isijinternational.30.699

[3] Hirano, T., Yamada, T. "Multi paradigm expert system architecture based upon the inverse design concept", In: Proceedings of the International Workshop on Artificial Intelligence for Industrial Applications, Hitachi City, Japan, 1988, pp. 245–250.
https://doi.org/10.1109/AIIA.1988.13301

[4] Murin, J., Aminbaghai, M., Hrabovsky, J., Gogola, R., Kugler, S. "Beam finite element for modal analysis of FGM structures", Engineering Structures, 121, pp. 1–18, 2016.
https://doi.org/10.1016/j.engstruct.2016.04.042

[5] Yoon, K., Lee, P.-S., Kim, D.-N. "Geometrically nonlinear finite element analysis of functionally graded 3D beams considering warping effects", Composite Structures, 132, pp. 1231–1247, 2015.
https://doi.org/10.1016/j.compstruct.2015.07.024

[6] Khebizi, M., Guenfoud, M. "Modélisation numérique des pouters FGM en utilisant la solution tridimensionnelle de Saint-Venant" (Numerical modeling of FGM beams using Saint-Venant's three-dimensional solution), presented at National Meetings of Civil Engineering and Hydraulics, Skikda, Algeria, Nov, 26–28, 2019.

[7] Khebizi, M., Guenfoud, M., Guenfoud, H. "Contribution à l'étude du comportement statique des poutres composites sandwichs par l'utilisation de la théorie de Saint-Venant" (Contribution to the study of the static behavior of sandwich composite beams using the Saint-Venant theory), presented at The 1st international Congress on Advances in Geotechnical Engineering and Construction Management (ICAGECM'2019), Skikda, Algeria, Dec, 9–10, 2019.

[8] Tsukamoto, H. "Mechanical properties of zirconia–titanium composites", International Journal of Materials Science and Applications, 3(5), pp. 260–267, 2014.
https://doi.org/10.11648/j.ijmsa.20140305.28

[9] Lee, Y.-H., Bae, S.-I., Kim, J.-H. "Thermal buckling behavior of functionally graded plates based on neutral surface", Composite Structures, 137, pp. 208–214, 2016.
https://doi.org/10.1016/j.compstruct.2015.11.023

[10] Goli, E., Kazemi, M. T. "XFEM modeling of fracture mechanics in transversely isotropic FGMs via interaction integral method", Procedia Materials Science, 3, pp. 1257–1262, 2014.
https://doi.org/10.1016/j.mspro.2014.06.204

[11] Rousseau, C.-E., Chalivendra, V. B., Tippur, H. V., Shukla, A. "Experimental fracture mechanics of functionally graded materials: an overview of optical investigations", Experimental Mechanics, 50(7), pp. 845–865, 2010.
https://doi.org/10.1007/s11340-010-9381-z

[12] Demirbas, M. D. "Thermal stress analysis of functionally graded plates with temperature-dependent material properties using theory of elasticity", Composites Part B: Engineering, 131, pp. 100–124, 2017.
https://doi.org/10.1016/j.compositesb.2017.08.005

[13] Chiba, R. "Stochastic thermal stresses in an FGM annular disc of variable thickness with spatially random heat transfer coefficients", Meccanica, 44(2), pp. 159–176, 2009
https://doi.org/10.1007/s11012-008-9158-y

[14] Yang, E. C., Zhao, X., Li, Y. H. "Free vibration analysis for cracked FGM beams by means of a continuous beam model", Shock and Vibration, 2015, 197049, 2015.
https://doi.org/10.1155/2015/197049

[15] Yang, J., Hao, Y. X., Zhang, W., Kitipornchai, S. "Nonlinear dynamic response of a functionally graded plate with a through-width surface crack", Nonlinear Dynamics, 59(1), pp. 207–219, 2010.
https://doi.org/10.1007/s11071-009-9533-9

[16] Elmeiche, A. "Analyse vibratoire des poutres en E-FGM" (Vibration analysis of E-FGM beams), [pdf] presented at CFM 2015,22ème Congrès Français de Mécanique (22nd French Congress of Mechanics), Lyon, France, Aug, 24–28, 2015. Available at: https://hal.archives-ouvertes.fr/hal-03446132/document

[17] Mahi, A., Bedia, E. A. A., Tounsi, A. "A new hyperbolic shear deformation theory for bending and free vibration analysis of isotropic, functionally graded, sandwich and laminated composite plates", Applied Mathematical Modelling, 39(9), pp. 2489–2508, 2015.
https://doi.org/10.1016/j.apm.2014.10.045

[18] Paul, A., Das, D. "Free vibration analysis of pre-stressed FGM Timoshenko beams under large transverse deflection by a variational method", Engineering Science and Technology, an International Journal, 19(2), pp. 1003–1017, 2016.
https://doi.org/10.1016/j.jestch.2015.12.012

[19] Ziou, H., Guenfoud, H., Guenfoud, M. "Numerical modelling of a Timoshenko FGM beam using the finite element method", International Journal of Structural Engineering, 7(3), pp. 239–261, 2016.
https://doi.org/10.1504/IJSTRUCTE.2016.077719

[20] Li, X.-F., Wang, B.-L., Han, J.-C. "A higher-order theory for static and dynamic analyses of functionally graded beams", Archive of Applied Mechanics, 80(10), pp. 1197–1212, 2010.
https://doi.org/10.1007/s00419-010-0435-6

[21] Vo, T. P., Thai, H.-T., Nguyen, T.-K., Inam, F., Lee, J. "Static behaviour of functionally graded sandwich beams using a Quasi-3D theory", Composites Part B: Engineering, 68, pp. 59–74, 2015.
https://doi.org/10.1016/j.compositesb.2014.08.030

[22] Nguyen, H. N., Hong, T. T., Vinh, P. V., Thom, D. V. "An efficient beam element based on Quasi-3D theory for static bending analysis of functionally graded beams", Materials, 12(13), 2198, 2019.
https://doi.org/10.3390/ma12132198

[23] Chikh, A. "Analysis of static behavior of a P-FGM Beam", [pdf] Journal of Materials and Engineering Structures, 6(4), pp. 513-524, 2019. [online] https://revue.ummto.dz/index.php/JMES/article/viewFile/2062/pdf

[24] Khebizi, M., Guenfoud, H., Guenfoud, M., El Fatmi, R. "Three-dimensional modelling of functionally graded beams using Saint-Venant", Structural Engineering and Mechanics, 72(2), pp. 257–273, 2019.
https://doi.org/10.12989/sem.2019.72.2.257

[25] Guendouz, I., Guenfoud, H., Guenfoud, M., Khebizi, M., Elfatmi, R. "Bending-torsional behavior analysis using a refined beam theory", Academic Journal of Civil Engineering, 39(1), pp. 59–62, 2021.
https://doi.org/10.26168/ajce.39.1.13

[26] Boumezbeur, K., Khebizi, M., Guenfoud, M. "Finite element modeling of static and cyclic response of functionality graded material beams", Asian Journal of Civil Engineering, 24(2), pp. 579–591, 2023.
https://doi.org/10.1007/s42107-022-00519-8

[27] Bhandari, M., Sharma, N. "Thermomechanical Solutions for Functionally Graded Beam subject to various Boundary Conditions", International Journal of Emerging Trends in Engineering Research, 8(5), pp. 1586–1591, 2020.
https://doi.org/10.30534/ijeter/2020/18852020

[28] Althoey, F., Ali, E. "A simplified stress analysis of functionally graded beams and influence of material function on deflection", Applied Sciences, 11(24), 11747, 2021.
https://doi.org/10.3390/app112411747

[29] Nguyen, V. X., Nguyen, K. T., Thai, S. "Large deflection analysis of functionally graded beams based on geometrically exact three-dimensional beam theory and isogeometric analysis", International Journal of Non-Linear Mechanics, 146, 104152, 2022.
https://doi.org/10.1016/j.ijnonlinmec.2022.104152

[30] Guendouz, I., Khebizi, M., Guenfoud, H., Guenfoud, M. "Analysis of FGM Cantilever Beams under Bending-torsional Behavior Using a Refined 1D Beam Theory", Periodica Polytechnica Civil Engineering, 66(4), pp. 1262–1277, 2022.
https://doi.org/10.3311/PPci.20595

[31] Guendouz, I., Khebizi, M., Guenfoud, H., Guenfoud, M., El Fatmi, R. "Analysis of torsional-bending FGM beam by 3D Saint-Venant refined beam theory", Structural Engineering and Mechanics, 84(3), pp. 423–435, 2022.
https://doi.org/10.12989/SEM.2022.84.3.423

[32] Zenkour, A. M., Sobhy, M. "Axial magnetic field effect on wave propagation in bi-layer FG graphene platelet-reinforced nanobeams", Engineering with Computers, 38(S2), pp. 1313–1329, 2022.
https://doi.org/10.1007/s00366-020-01224-3

[33] Giunta, G., Belouettar, S., Carrera, E. "Analysis of FGM beams by means of classical and advanced theories", Mechanics of Advanced Materials and Structures, 17(8), pp. 622–635, 2010.
https://doi.org/10.1080/15376494.2010.518930

[34] Zghal, S., Ataoui, D., Dammak, F. "Static bending analysis of beams made of functionally graded porous materials", Mechanics Based Design of Structures and Machines, 50(3), pp. 1012–1029, 2022.
https://doi.org/10.1080/15397734.2020.1748053

[35] Guenfoud, H., Ziou, H., Himeur, M., Guenfoud, M. "Analyses of a composite functionally graded material beam with a new transverse shear deformation function", Journal of Applied Engineering Science & Technology, 2(2), pp. 105–113, 2016.

[36] Hadji, L., Daouadji, T. H., Meziane, M. A. A., Tlidji, Y., Bedia, E. A. A. "Analysis of functionally graded beam using a new first-order shear deformation theory", Structural Engineering and Mechanics, 57(2), pp. 315–325, 2016.
https://doi.org/10.12989/sem.2016.57.2.315

[37] Delale, F., Erdogan, F. "The crack problem for a nonhomogeneous plane", Journal of Applied Mechanics, 50(3), pp. 609–614, 1983.
https://doi.org/10.1115/1.3167098

[38] Ben-Oumrane, S., Abedlouahed, T., Ismail, M., Mohamed, B. B., Mustapha, M., El Abbas, A. B. "A theoretical analysis of flexional bending of Al/Al2O3 S-FGM thick beams", Computational Materials Science, 44(4), pp. 1344–1350, 2009.
https://doi.org/10.1016/j.commatsci.2008.09.001

[39] Dhondt, G. "The finite element method for three-dimensional thermomechanical applications", John Wiley & Sons, 2004. ISBN: 0-470-85752-8
https://doi.org/10.1002/0470021217

[40] Smith, M. "ABAQUS/Standard User's Manual, Version 6.11", Dassault Systèmes Simulia Corp, 2011.

[41] Zafarmand, H., Kadkhodayan, M. "Nonlinear material and geometric analysis of thick functionally graded plates with nonlinear strain hardening using nonlinear finite element method", Aerospace Science and Technology, 92, pp. 930–944, 2019.
https://doi.org/10.1016/j.ast.2019.07.015

[42] Liew, K. M., Rajendran, S. "New superconvergent points of the 8-node serendipity plane element for patch recovery", International Journal for Numerical Methods in Engineering, 54(8), pp. 1103–1130, 2002.
https://doi.org/10.1002/nme.460